Circularly Polarized X Rays as a Probe of Noncollinear Magnetic Order in Multiferroic TbMnO$_3$

F. Fabrizi,[1,2] H. C. Walker,[1,2,*] L. Paolasini,[1] F. de Bergevin,[1] A. T. Boothroyd,[3] D. Prabhakaran,[3] and D. F. McMorrow[2]

[1]*European Synchrotron Radiation Facility (ESRF), Boîte Postale 220, 38043 Grenoble, France*
[2]*London Centre for Nanotechnology and Department of Physics and Astronomy, University College London,*
Gower Street, London WC1E 6BT, United Kingdom
[3]*Department of Physics, Clarendon Laboratory, University of Oxford, United Kingdom*

Nonresonant x-ray magnetic scattering has been used to study the magnetic structure of multiferroic TbMnO$_3$ in its ferroelectric phase. Circularly polarized x rays were combined with full polarization analysis of the scattered beam to reveal important new information on the magnetic structure of this canonical multiferroic. An applied electric field is shown to create essentially a single magnetic domain state in which the cycloidal order on the Mn sublattice rotates either clockwise or anticlockwise depending on the sign of the field. It is demonstrated how this technique provides sensitivity to the absolute sense of rotation of the Mn moments and to components of the ordering on the Tb sublattice and phase shifts that earlier neutron diffraction experiments could not resolve.

PACS numbers: 75.25.+z, 61.05.cp, 75.50.Ee

Multiferroic materials exhibit unusual physical properties as a result of coupling between the various forms of spontaneous ferroic order they display [1]. Recently, considerable interest has been generated following the discovery of a large magnetoelectric coupling in TbMnO$_3$ [2], which was subsequently shown to be due to the establishment of noncollinear antiferromagnetic order driving the formation of a ferroelectric (FE) state [3]. A central theme of ensuing studies in TbMnO$_3$ and other systems has been to explore the electric field control of magnetism and correspondingly the magnetic field control of the FE state [4,5]. Of paramount importance in the development of any theory of the magnetoelectric coupling in this class of materials is a complete and accurate microscopic description of the magnetic structures they display.

Historically, the utility of circularly polarized (CP) x rays is well established in dichroism experiments on ferromagnets [6–8]. Less attention has been paid to the case of antiferromagnets, with even fewer examples of the use of CP x rays in diffraction from noncollinear systems such as helices and cycloids [9,10]. Here we report on a new application of CP x rays in combination with full polarimetry of the scattered beam to the refinement of magnetic structures in magnetoelectric multiferroics. Besides the classical advantages provided by x-ray magnetic diffraction (including discrimination between spin and orbital contribution, in nonresonant scattering) [11], we demonstrate how this technique provides unique insight into the formation of cycloidal domains in TbMnO$_3$. A key feature of these experiments was the control of the population of magnetic domains by an applied electric field.

Bulk measurements first established that TbMnO$_3$ undergoes a transition below $T = 27$ K to a multiferroic state that is both magnetic and FE and demonstrated how a magnetic field could be used to control ferroelectricity [2].

A major breakthrough in understanding this effect was provided by a neutron diffraction study which concluded that at $T = 27$ K the Mn $3d$ magnetic moments undergo a transition from a collinear to a noncollinear, cycloidal phase, described by an incommensurate wave vector $\mathbf{k}_m = \tau\mathbf{b}^*$, which removes a center of inversion so as to form a FE state [3]. For this class of multiferroic, the FE moment $\mathbf{P}$ may be conveniently written as $\mathbf{P} \propto \mathbf{k}_m \times \mathbf{C}$, where $\mathbf{C} = \sum_i \mathbf{S}_i \times \mathbf{S}_{i+1}$ characterizes the magnetic structure adopted by the spins $\mathbf{S}_i$ [12–14]. In the case of TbMnO$_3$, the Mn magnetic moments in the cycloidal phase rotate in the **b**-**c** plane [Fig. 1(b)], and with $\mathbf{k}_m$ parallel to the **b** axis, $\mathbf{P}$ is either parallel or antiparallel to the **c** axis depending on the sign of $\mathbf{C}$. The same study [3] proposed that the Tb $4f$ moments are also sinusoidally modulated at $\mathbf{k}_m$ but are transversely polarized along the **a** axis. Polarized neutron diffraction has recently been applied to multiferroics [15,16], including TbMnO$_3$ [17], where it was found that the cycloid could be switched from propagating clockwise or anticlockwise, depending on the direction of the applied electric field [17]. Our nonresonant x-ray magnetic scattering (NRXMS) study of TbMnO$_3$ establishes the utility of x rays for studying the electric field control of magnetism in multiferroics. Although NRXMS experiments are in many ways much more demanding than neutron diffraction, due to the extreme weakness ($\sim 10^{-5}$–10^{-7}) of the NRXMS relative to the charge scattering, they are nonetheless of considerable value due to the complementary nature of the information they provide. In the case of TbMnO$_3$, this has allowed us to reveal the ordering of a b component on the Tb sublattice and to determine various phase relationships that were hitherto unknown.

TbMnO$_3$ adopts the *Pbnm* space group [Fig. 1(a)] at room temperature with $a_0 = 5.302$ Å, $b_0 = 5.856$ Å, and $c_0 = 7.400$ Å [18]. We selected a single crystal grown by
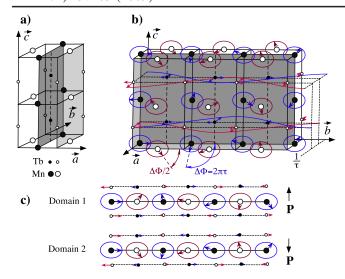
FIG. 1 (color online).   (a) Crystallographic and (b) magnetic structures of TbMnO$_3$. The incommensurate magnetic structure propagates along the **b** direction with periodicity $1/\tau b_0 \approx 3.55 b_0$ on both the Mn and Tb sublattices. Both the transverse and the previously undetermined longitudinal components of the Tb moments are shown. (c) Projection in the **b-c** plane of the two cycloidal magnetic domains, also showing the newly determined longitudinal Tb moment component. Domain 1 (2) is favored by electric field **E** > 0 (**E** < 0) (see Fig. 3).

the floating zone method, as used in previous x-ray resonant scattering experiments [19,20]. The sample had dimensions $2 \times 2 \times 0.8$ mm^3, and a poling electric field **E** of about 1 kV/mm was applied during the cooling procedure inside a ^{4}He evaporation cryostat. Two copper electrodes were glued using highly conductive silver paste on the (001) surfaces of the sample [Fig. 2(a)]. The electric field was removed during the x-ray experiments.

X-ray magnetic diffraction experiments were performed at the ID20 beam line [21] (ESRF, Grenoble, France) using a monochromatic beam at a wavelength of $\lambda = 1.66$ Å, so as to excite nonresonant processes, which allows the spin and orbital magnetizations to be determined independently [22]. (Neutron scattering, by contrast, is sensitive to their sum.) Linearly polarized x rays were converted into left-circularly polarized (LCP) or right-circularly polarized (RCP) photons using a diamond quarter-wave plate (circular polarization typically 99%) or allowed to pass unchanged through the phase plate; see Fig. 2(a). For a cycloidal magnet, the incoming circular polarization finds its handedness naturally coupled to the sense of rotation of the magnetic moments, allowing the population of domains to be determined by observing differences in the intensity of magnetic diffraction peaks under illumination with LCP or RCP x rays. An Au (222) crystal analyzer system mounted on the detector arm of a six-circle diffractometer was used to characterize the polarization of the scattered photons. The polarization is represented by the Stokes vector $\mathbf{P} = (P_1, P_2, P_3)$ [22,23], whose linear components P_1 and P_2 were determined by fitting the dependence of the
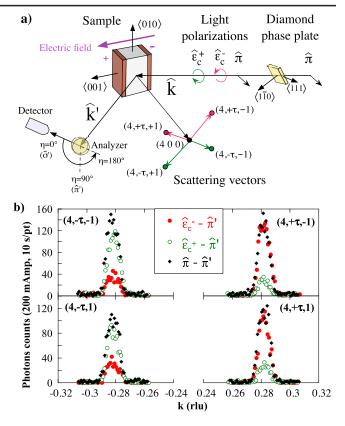

FIG. 2 (color online).   (a) Schematic of experimental scattering geometry used to determine the polarization dependence of A-type magnetic satellite reflections $(4, \pm\tau, \pm1)$ in TbMnO$_3$. (b) Incident polarization dependence of these reflections in the FE cycloidal phase at 15 K, obtained after annealing the sample with **E** < 0. The polarization of the scattered photons was analyzed in the $\hat{\pi}'$ channel ($\eta = 90°$).

scattered x-ray intensity $I(\eta) = I_0 (1 + P_1 \cos 2\eta + P_2 \sin 2\eta)$ on the angle η of the polarization analyzer about the wave vector $\mathbf{k}'$. The Stokes parameters of the incident beam were carefully checked before and after every set of scans using the polarization analyzer, to control the incident circular photon polarization, which is very sensitive to the stability of the beam.

The initial objective of our study was to establish whether or not our experimental setup provided sufficient sensitivity to any imbalance in the population of magnetic domains produced by the applied **E** field. Figure 2(b) shows the polarization dependence of the scattering from the four A-type [24] $(4, \pm\tau, \pm1)$ magnetic satellite reflections—each satellite forming one arm of the so-called star of wave vectors around $(4, 0, 0)$. The measurements were performed at 15 K in the FE phase, after cooling the sample with a poling voltage of -700 V. Data were collected with linear ($\hat{\pi}$, black diamonds), RCP ($\hat{\epsilon}_c^+$, open green circles), and LCP ($\hat{\epsilon}_c^-$, red filled circles) polarized x rays, while the scattered beam was analyzed in the $\hat{\pi}'$ channel ($\eta = 90°$). Inspection of Fig. 2(b) reveals that the intensities of the magnetic satellites are very similar when incident linear polarization $\hat{\pi}$ is selected. For incident circular polariza-

tions, this is not the case: instead, the intensities display complementary behavior, depending on the sign of τ. In the case of equipopulated cycloidal domains the intensities associated with $\hat{e}_c^+$ and $\hat{e}_c^-$ should be similar, whereas for a single cycloidal domain a large difference is expected, as is indeed observed to be the case.

The standard approach to obtain a microscopic understanding of the magnetic structure would be to collect intensity data for a set of satellites $(h, k \pm \tau, l)$ with (hkl) taking on as wide a range of values as possible. The disadvantages of this method are that large corrections must be applied for effects such as absorption, etc., and that our specific scattering geometry restricts the accessible (hkl) values. Instead, we undertook a detailed analysis of the polarization of the scattered beam by carefully measuring $I(\eta)$ for each of the satellites shown in Fig. 2(a), allowing us to extract the Stokes parameters. Figure 3 summarizes our data for field coolings performed with either $\mathbf{E} > 0$ or $\mathbf{E} < 0$. The data were obtained by rocking the crystal analyzer at different η angles and are normalized by monitor and corrected by subtraction of the background.

Turning first to consider the case of incident linear ($\hat{\pi}$) polarization shown in Fig. 3, it is clear that, for a particular choice of the direction of $\mathbf{E}$, only small differences in $I(\eta)$ are observed for the various satellites and that reversing the direction of $\mathbf{E}$ does not appear to have any effect. Clear
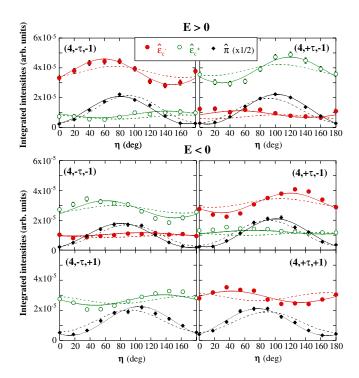

FIG. 3 (color online). Variation with analyzer rotation angle η of the x-ray magnetic scattering in TbMnO$_3$ at 15 K, for field cooling with either $\mathbf{E} > 0$ (upper panel) or $\mathbf{E} < 0$ (lower panel). The dashed lines represent the model described in Ref. [3], whereas the continuous lines are our model calculations, as described in the text.

differences in $I(\eta)$ of the various satellites are observed for incident circular polarization. In this case, reversing the direction of $\mathbf{E}$ has a profound effect on the observed intensities. For a given field direction, changing the sign of τ at fixed l leads to a switching of the handedness of incident x rays that produces the maximum intensity, whereas the handedness associated with the maximum satellite intensity is invariant with respect to changes in the sign of l. Of considerable significance is the fact that reversing the sign of $\mathbf{E}$ leads to a switching of the dominant handedness. Also apparent are clear mirror symmetries between LCP and RCP x rays for the same reflection and between $\pm l$ satellites for the same incident polarization state. Thus at a qualitative level the data displayed in Fig. 3 reveal an imbalance in the population of the two possible magnetic domains created by the applied electric field, an imbalance that can be reversed by switching the direction of the field.

To explore the potential richness of information encoded in the data shown in Fig. 3, we performed extensive modeling of the magnetic scattering. For the initial model we used the structure of Blasco *et al.* [18], as shown in Fig. 1(a), and the magnetic structure proposed by Kenzelmann *et al.* [3], as shown in Fig. 1(b). In Fig. 3, the results of our calculations of NRXMS [22] based on this model are represented by dashed lines. For the calculations, the exact scattering geometry of the six-circle setup was taken into account. The agreement between the model and the data is clearly unsatisfactory. In particular, the data show a nonzero value of P_2 (a linear polarization oblique with respect to the $\hat{\sigma}'$ and $\hat{\pi}'$ directions) that is not predicted by the model.

A vastly improved description of the data was achieved following the realization that, in contrast to the earlier neutron diffraction study, our experiment yielded sensitivity to the b component of the ordered moment on the Tb sites, while being largely insensitive to the a component. From the fits, we are able to fix the phase angle between the magnetic modulations of the Tb and the Mn atoms. Consider one Mn atom and the subsequent Tb atom moving along $\pm\mathbf{c}$ (sign determined according to the direction of the electric polarization), and then the phase angle between their magnetic modulations, evaluated at the same coordinate in space, is found to be $1.0 \pm 0.1\pi$ (with reference to the b components). The phase shift between the two orbits of Tb atoms (at fractional coordinates $z = 1/4$ and $3/4$) is determined to be $1.0 \pm 0.2\pi$.

The model results in the following NRXMS amplitude for an A-type peak of the form $(4, \pm\tau, \pm1)$:

$$f(\mathbf{K}) \propto [S_b^{\mathrm{Mn}}(\mathbf{K})\hat{\mathbf{b}} - \gamma\alpha i S_c^{\mathrm{Mn}}(\mathbf{K})\hat{\mathbf{c}}] \cdot \mathbf{B}$$
$$- \gamma\beta i [S_b^{\mathrm{Tb}}(\mathbf{K})\hat{\mathbf{b}} \cdot \mathbf{B} + \tfrac{1}{2}L_b^{\mathrm{Tb}}(\mathbf{K})\hat{\mathbf{b}} \cdot \mathbf{A}''] \cos(8\pi\Delta_a^{\mathrm{Tb}}),$$

where the value of $\alpha = \pm1$ selects the sign of τ and β the sign of $l = \pm1$ and $\gamma = \pm1$ identifies the two cycloidal domains 1 and 2, respectively [Fig. 1(c)]. The vectors $\mathbf{A}''$ and $\mathbf{B}$ contain the dependence on the polarization of the

incident and diffracted x rays [22]. The spin $S_i^X(\mathbf{K})$ and the orbital $L_i^X(\mathbf{K})$ magnetic components contain the form factors for $X = \text{Mn}^{3+}$ and Tb^{3+} at a given scattering vector $\mathbf{K}$. We suppose also that the orbital contribution of the Mn ions is quenched, and that of Tb is equal to its spin moment ($L^{\text{Tb}}/S^{\text{Tb}} = 1$) as follows from Hund's rules for a $^7F_6$ electronic configuration. Finally, Δ_a^{Tb} describes the fractional atomic coordinate along the **a** axis of the Wyckoff position (4c) occupied by the Tb atoms [18].

A simplified expression for the NRXMS amplitude in the $\hat{\sigma}'$ and $\hat{\pi}'$ channels, in which we set the scattering angle $2\theta = 90°$, $\Delta_a^{\text{Tb}} = 0$, and place the **b** axis perpendicular to the scattering plane, illustrates the sensitivity in our experiment to the different components of the Tb and Mn magnetic moments and the dependence of the scattered intensity on the handedness of the x rays, etc.:

$$f_{\hat{\sigma}'} \propto S_b^{\text{Mn}} + \epsilon \alpha \gamma S_c'^{\text{Mn}} - i\beta\gamma S_b^{\text{Tb}},$$

$$f_{\hat{\pi}'} \propto (\epsilon\beta\gamma)(S_b^{\text{Tb}} + L_b^{\text{Tb}}) + i(\epsilon S_b^{\text{Mn}} + \alpha\gamma S_c^{\text{Mn}}).$$

Here ϵ selects the handedness of the incident x rays, and $S_c^{(\prime)\text{Mn}}$, etc., are the projected magnetization densities on the incident (scattered) wave vector. The dominant Mn terms are real in $f_{\hat{\sigma}'}$ and imaginary in $f_{\hat{\pi}'}$, giving a scattered beam that is mainly circularly polarized. They are large (small) if $\epsilon\alpha\gamma = +1$ (-1). A nonzero value of P_2 arises when the pair $f_{\hat{\sigma}'} \pm f_{\hat{\pi}'}$ have different moduli. This depends on S_b^{Tb} and L_b^{Tb}. Their sign in $f_{\hat{\pi}'}$ ($f_{\hat{\sigma}'}$) is to be compared to the sign of the largest term S_b^{Mn} in $f_{\hat{\sigma}'}$ ($f_{\hat{\pi}'}$). Then it is seen that S_b^{Tb} adds with opposite signs in the real and imaginary parts, so that its effect in P_2 nearly cancels. Instead, L_b^{Tb} produces a net P_2 of sign $+\epsilon\beta\gamma$.

The full expression for $f(\mathbf{K})$ was fitted to the data with the outcome represented by the solid lines in Fig. 3. It is clear that inclusion of a b component of the Tb moment leads to an excellent description of the data, with the best fit obtained with ($L_b^{\text{Tb}} + 2S_b^{\text{Tb}}$) equal to $1.0 \pm 0.3\mu_B$. Most importantly, our refined model of the magnetic structure allows us to obtain an accurate description of the domain state in our sample as a function of applied electric field, including the absolute sense of rotation of the magnetic moments. We conclude that cooling in a positive electric field led to a population of 96(3)% of the cycloidal domain in which the transverse spiral of the Mn atoms is anticlockwise, when moving along $+\mathbf{b}$ and looking from $+\mathbf{a}$ [domain 1 in Fig. 1(c)], while field cooling in a negative electric field produced a population of 83(2)% for the domain of the opposite sense of rotation [domain 2 in Fig. 1(c)]. Differences in the domain populations found with $\pm\mathbf{E}$ may result from a number of effects such as domain pinning, slight variations in the volume probed by the x-ray beam, etc.

Our results establish the benefits of performing NRXMS experiments when circularly polarized x rays are combined with full polarization analysis of the scattered beam. Applied to cycloidal systems, this technique is capable of providing a quantitative, microscopic description of the cycloidal domain state. For the specific case of multiferroic TbMnO_3, with two different types of magnetic ion, making it by any standards a challenging test case, we have shown surprisingly that this approach allows us to make important refinements to the magnetic structure obtained from neutron diffraction. This technique could readily be applied to other multiferroics, particularly those such as BiFeO_3 [25,26] for which open questions remain concerning the magnetic structure of bulk samples and its modification in thin films [16,27–29].

---

*helen.walker@esrf.fr
[1] M. Fiebig, J. Phys. D **38**, R123 (2005).
[2] T. Kimura *et al.*, Nature (London) **426**, 55 (2003).
[3] M. Kenzelmann *et al.*, Phys. Rev. Lett. **95**, 087206 (2005).
[4] W. Eerenstein, N. D. Mathur, and J. F. Scott, Nature (London) **442**, 759 (2006).
[5] S.-W. Cheong and M. Mostovoy, Nature Mater. **6**, 13 (2007).
[6] J. Erskine and E. Stern, Phys. Rev. B **12**, 5016 (1975).
[7] G. van der Laan *et al.*, Phys. Rev. B **34**, 6529 (1986).
[8] G. Schütz *et al.*, Phys. Rev. Lett. **58**, 737 (1987).
[9] C. Sutter *et al.*, Phys. Rev. B **55**, 954 (1997).
[10] H. A. Durr *et al.*, Science **284**, 2166 (1999).
[11] L. Paolasini and F. de Bergevin, C.R. Physique **9**, 550 (2008).
[12] H. Katsura, N. Nagaosa, and A. V. Balatsky, Phys. Rev. Lett. **95**, 057205 (2005).
[13] M. Mostovoy, Phys. Rev. Lett. **96**, 067601 (2006).
[14] I. A. Sergienko, C. Şen, and E. Dagotto, Phys. Rev. Lett. **97**, 227204 (2006).
[15] P. G. Radaelli *et al.*, Phys. Rev. Lett. **101**, 067205 (2008).
[16] S. Lee *et al.*, Phys. Rev. B **78**, 100101(R) (2008).
[17] Y. Yamasaki *et al.*, Phys. Rev. Lett. **98**, 147204 (2007).
[18] J. Blasco *et al.*, Phys. Rev. B **62**, 5609 (2000).
[19] D. Mannix *et al.*, Phys. Rev. B **76**, 184420 (2007).
[20] T. R. Forrest *et al.*, J. Phys. Condens. Matter **20**, 422205 (2008).
[21] L. Paolasini *et al.*, J. Synchrotron Radiat. **14**, 301 (2007).
[22] M. Blume and D. Gibbs, Phys. Rev. B **37**, 1779 (1988).
[23] F. de Bergevin and M. Brunel, Acta Crystallogr. Sect. A **37**, 314 (1981).
[24] S. Quezel *et al.*, Physica (Amsterdam) **86B+C–88B+C**, 916 (1977).
[25] J. R. Teague, R. Gerson, and W. J. James, Solid State Commun. **8**, 1073 (1970).
[26] I. Sosnowska, T. P. Neumaier, and E. Steichele, J. Phys. C **15**, 4835 (1982).
[27] J. Wang *et al.*, Science **299**, 1719 (2003).
[28] C. Ederer and N. A. Spaldin, Phys. Rev. B **71**, 224103 (2005).
[29] T. Zhao *et al.*, Nature Mater. **5**, 823 (2006).